

Super-universality of eigenchannel structures and possible optical applications

Ping Fang,¹ Chushun Tian,^{1,*} Liyi Zhao,² Yury P. Bliokh,^{3,1,4} Valentin Freilikher,^{5,1,4} and Franco Nori^{4,6}

¹*CAS Key Laboratory of Theoretical Physics and Institute of Theoretical Physics, Chinese Academy of Sciences, Beijing 100190, China*

²*Institute for Advanced Study, Tsinghua University, Beijing 100084, China*

³*Department of Physics, Technion-Israel Institute of Technology, Haifa 32000, Israel*

⁴*Theoretical Quantum Physics Laboratory, RIKEN Cluster for Pioneering Research, Wako-shi, Saitama 351-0198, Japan*

⁵*Department of Physics, Bar-Ilan University, Ramat-Gan 52900, Israel*

⁶*Department of Physics, University of Michigan, Ann Arbor, Michigan 48109-1040, USA*

(Dated: December 15, 2024)

The propagation of waves through transmission eigenchannels in complex media is emerging as a new frontier of condensed matter and wave physics. A crucial step towards constructing a complete theory of eigenchannels is to demonstrate their spatial structure in any dimension and their wave-coherence nature. Here, we present new spatial properties of the radiation propagating in such channels in diffusive random media. We show that the transverse (with respect to the direction of propagation) intensity distribution depends on the aspect ratio of a sample. As the width of the sample increases, so that it transforms from quasi one-dimensional (1D) to two-dimensional (2D) geometry, the shape of the eigenvector of the transmission matrix (incoming signal) undergoes a delocalization-localization crossover, which results in the formation of a transverse-localized structure of the eigenchannel. As this takes place, the dependence on the longitudinal coordinate does not change and is given by the same analytical expression as that for quasi-1D. This expression is super-universal in the sense that, with a minimal modification, it describes also the spatial structures of localized resonances in strictly 1D random systems. A remarkable intrinsic property of the eigenchannels is that, notwithstanding the diffusive nature of the medium, a wave, being localized in the input remains so in the course of propagation along the entire sample. The obtained results suggest that despite the diversity of wave phenomena in different dimensions, the underlying physics of eigenchannels might include universal key ingredients, which are of 1D nature and are closely related to the resonances. Our findings open up a way to tailor the spatial energy density distribution in opaque materials.

I. INTRODUCTION

An unprecedented degree of control reached in experiments on classical waves is turning the dream of understanding and controlling wave propagation in complex media into reality¹. Central to many ongoing research activities is the concept of transmission eigenchannel^{2–10} (abbreviated as eigenchannel hereafter). Loosely speaking, the eigenchannel refers to a specific wave field, which is excited by the input waveform corresponding to the right-singular vector^{11–13} of the transmission matrix (TM) \mathbf{t} . When a wave is launched into a complex medium it is decomposed into a number of “partial waves”, each of which propagates along an eigenchannel and whose superposition gives the field distribution excited by the incoming wave. Thus, in contrast to the TM, which treats media as a black box and has been well studied¹⁴, eigenchannels are largely unexplored, in spite of the fact that these provide rich information about the properties of wave propagation in the interior of the media. The understanding of the spatial structures of these channels can provide a basis for both fundamentals and applications of wave physics in complex media.

Until recently, the emphasis has been placed on the structures of eigenchannels in quasi 1D disordered media^{3–8}. Yet, measurements of the three-dimensional spatial resolution of eigenchannels have recently been within experimental reach⁹. In addition, numerical

results¹⁰ have suggested that in high-dimensional media eigenchannels may exhibit intriguing structures which can carry some universalities that embrace quasi 1D eigenchannels as well. Thus to demonstrate how the eigenchannel structure evolves in the crossover from low to higher dimension, and to understand the underlying mechanism, it is not only of fundamental interests, but also important for obtaining better insights on the experimental results on the eigenchannel structures in higher dimension.

Another motivation of the present work comes from a recent surprising finding¹⁵ regarding a seemingly unrelated object, the resonance in layered disordered samples which, from the mathematical point of view, are strictly 1D systems. The resonance refers to a local maximum in the transmittance spectrum¹⁶, which has a natural connection to Anderson localization in 1D^{17,18} and resonators in various systems, ranging from plasmonics to metamaterials¹⁹. Despite the conceptual difference between the resonance and the eigenchannel, it was found¹⁵ that the distribution of resonant transmissions in the (i) 1D *Anderson localized* regime and (ii) the transmission eigenvalues in quasi-1D *diffusive* regime are exactly the same, namely, the bimodal distribution^{11,13}. However, the mechanism underlying this similarity remains unclear. Most importantly, it is of fundamental interest to understand whether this similarity is restricted only to transmissions, or can be extended to spatial structures.

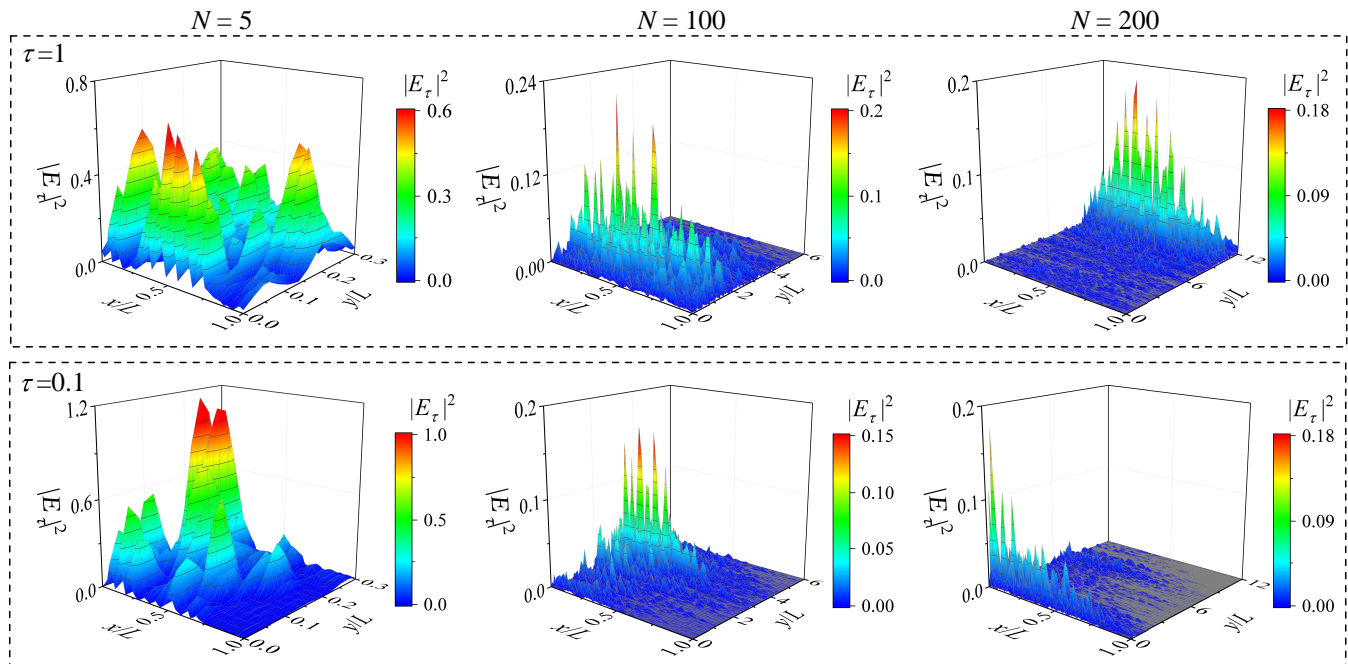


FIG. 1. Simulations show that as the width W increases, so that a quasi-1D ($N = 5$) waveguide turns into a 2D slab ($N = 100, 200$), the eigenchannel structure $|E_\tau(x, y)|^2$ (in a single disordered medium) exhibits a crossover from delocalization to localization in the transverse y direction. The eigenchannel structures in the upper (lower) panels correspond to the eigenvalue $\tau = 1$ ($\tau = 0.1$). For all panels the disorder strength is the same, and $L = 50$.

In this work we show that in a diffusive medium, as the transverse dimension of a sample (and consequently the number of channels) increases, the right-singular vectors of the TM undergo a delocalization-localization crossover, which triggers the formation of transverse-localized structures of eigenchannels. While this takes place, the depth profile of the energy density (integrated over the cross section) remains unaffected, and is given by precisely the same expression as that for quasi-1D found in Ref. 4.

We also study the spatial structures of resonance in strictly 1D. We find that they have a universal analytic expression, which is similar to that for eigenchannel structures and the modifications are minimal. Our findings may serve as a proof of the conjecture² of the eigenchannel structure–Fabry-Perot cavity analogy.

The remainder of this paper is organized as follows. In Sec. II, we introduce some basic concepts of eigenchannels and resonances. In Sec. III, we study in detail how the eigenchannel structure in a diffusive medium evolves as the medium crosses over from quasi-1D to a higher-dimensional slab geometry. To be specific, throughout this work we focus on two-dimensional (2D) samples. In Sec. IV, we study in detail the spatial structure of 1D resonances. In Sec. V, possible optical applications are discussed. In Sec. VI, we conclude and discuss the results.

II. EIGENCHANNEL AND RESONANCE: BASIC CONCEPTS

To introduce the concept of eigenchannels^{1,2,4}, we consider the transmission of a monochromatic wave (with circular frequency Ω) through a rectangular ($0 \leq x \leq L, 0 \leq y \leq W$) diffusive dielectric medium bounded in the transverse (y) direction by reflecting walls at $y = 0$ and $y = W$. For $W \gtrsim L$ ($W \ll L$) the medium geometry is 2D (quasi 1D). The wave field $E(x, y)$ satisfies the Helmholtz equation, (the velocity of waves in the background is set to unity)

$$\{\partial_x^2 + \partial_y^2 + \Omega^2 [1 + \delta\epsilon(x, y)]\} E(x, y) = 0, \quad (1)$$

where $\delta\epsilon(x, y)$ is a random function, which presents the fluctuations of the dielectric constant inside the sample, and equals zero at $x < 0$ and $x > L$. To study the evolution of the eigenchannel structure in the crossover from quasi-1D to 2D, we increase W and keep L, Ω and the strength of disorder fixed.

The incoming and transmitted current amplitudes are related to each other by the transmission matrix $\mathbf{t} \equiv \{t_{ab}\}$, where a, b label the ideal (i.e., $\delta\epsilon(x, y) = 0$) waveguide modes $\varphi_a(y)$. The matrix elements are

$$t_{ab} = -i\sqrt{\tilde{v}_a \tilde{v}_b} \langle x = L, a | G | x' = 0, b \rangle, \quad (2)$$

where G is the retarded Green's function associated with the Helmholtz equation, and \tilde{v}_a is the group velocity of mode a .

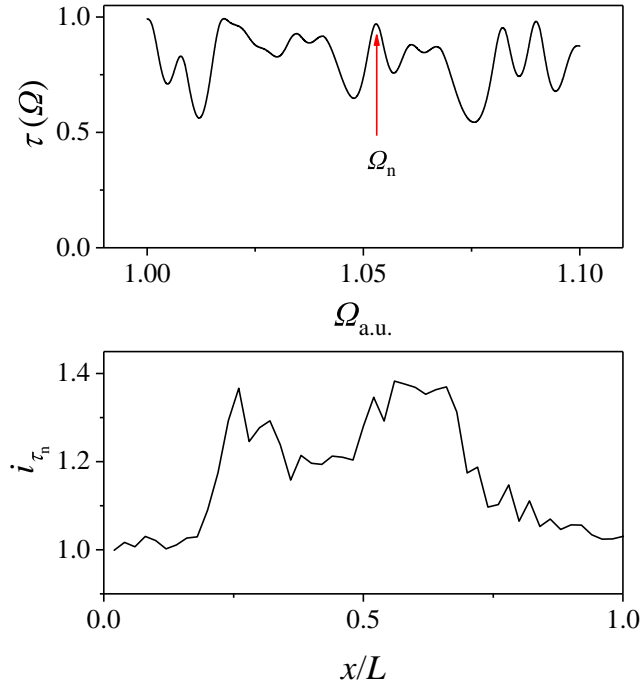


FIG. 2. Example of a transmittance spectrum $\mathcal{T}(\Omega)$ (top) and the resonance structure $\tilde{I}_{\mathcal{T}_n}(x)$ corresponding to the resonant frequency Ω_n (bottom).

The matrix \mathbf{t} is non-hermitian, thus we perform its singular value decomposition, i.e.,

$$\mathbf{t} = \sum_{n=1}^N \mathbf{u}_n \sqrt{\tau_n} \mathbf{v}_n^\dagger, \quad (3)$$

to find the singular value τ_n and the corresponding left (right)-singular vector \mathbf{v}_n (\mathbf{u}_n) normalized to unity. The input waveform \mathbf{v}_n uniquely determines the so-called transmission eigenchannel labeled by n , over which radiation propagates in a random medium^{1,2,4}, and τ_n gives the transmission coefficient of the n th eigenchannel and is also called the transmission eigenvalue. Importantly, the total transmittance is the sum over all transmission eigenvalues, $\sum_n \tau_n$. Moreover, many statistical properties of transport through random media such as the fluctuations and correlations of conductance and transmission may be described in terms of the statistics of the transmission eigenvalues⁴.

To find the spatial structure of eigenchannels, we replace $x = L$ in Eq. (2) by arbitrary $x \in [0, L)$, which yields:

$$t_{ab} \rightarrow t_{ab}(x) \equiv -i\sqrt{\bar{v}_a \bar{v}_b} \langle x, a | G | x' = 0, b \rangle. \quad (4)$$

From this we obtain the field distribution inside the medium,

$$\mathbf{E}_{\tau_n}(x) \equiv \{E_{na}(x)\} = \mathbf{t}(x)\mathbf{v}_n, \quad (5)$$

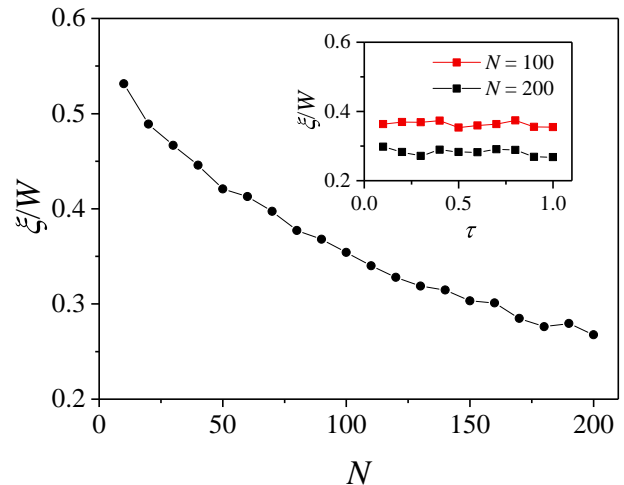


FIG. 3. Simulations show that for a given width $N \propto W$, the participation ratio $\xi(\tau)$ is approximately independent of the transmission coefficient τ (inset), where $\xi(\tau)$ is computed by using Eq. (10) and averaged over 100 right-singular vectors of same singular values: namely, transmission eigenvalues in distinct statistically equivalent disorder configurations. Simulations further show that as W increases, while other conditions stay the same, the ratio of ξ'/W has a tendency of decreasing to zero (main panel). Here ξ' is computed by using Eq. (11) and the average is over 1000 right-singular vectors of distinct eigenvalues in statistically equivalent disorder configurations.

excited by the input field \mathbf{v}_n which is the right-singular vector of the TM. Changing from the ideal waveguide mode (φ_a) representation to the coordinate (x, y) representation gives a specific 2D spatial structure, namely, the energy density profile:

$$|\mathbf{E}_{\tau_n}(x, y)|^2 = \left| \sum_{a=1}^N E_{na}(x) \varphi_a^*(y) \right|^2, \quad (6)$$

which defines the 2D eigenchannel structure associated with the transmission eigenvalue τ_n . Examples of this 2D structure are given in Fig. 1. Integrating Eq. (6) over the transverse coordinate y we obtain the depth profile of the energy density of the n -th eigenchannel,

$$w_{\tau_n}(x) \equiv \int dy |\mathbf{E}_{\tau_n}(x, y)|^2, \quad (7)$$

which is a key quantity to be addressed below. It is important that, in the definitions of (6) and (7), the frequency Ω is fixed.

To proceed, we present a brief review of resonances in media with one-dimensional disorder (cf. Fig. 2). For a detailed introduction we refer to Ref. 19. In the strictly 1D case, the wave field $E_\Omega(x)$ satisfies [like in Eq. (1) the velocity of waves in the background is set to unity.]

$$\{\partial_x^2 + \Omega^2 [1 + \delta\epsilon(x)]\} E_\Omega(x) = 0, \quad (8)$$

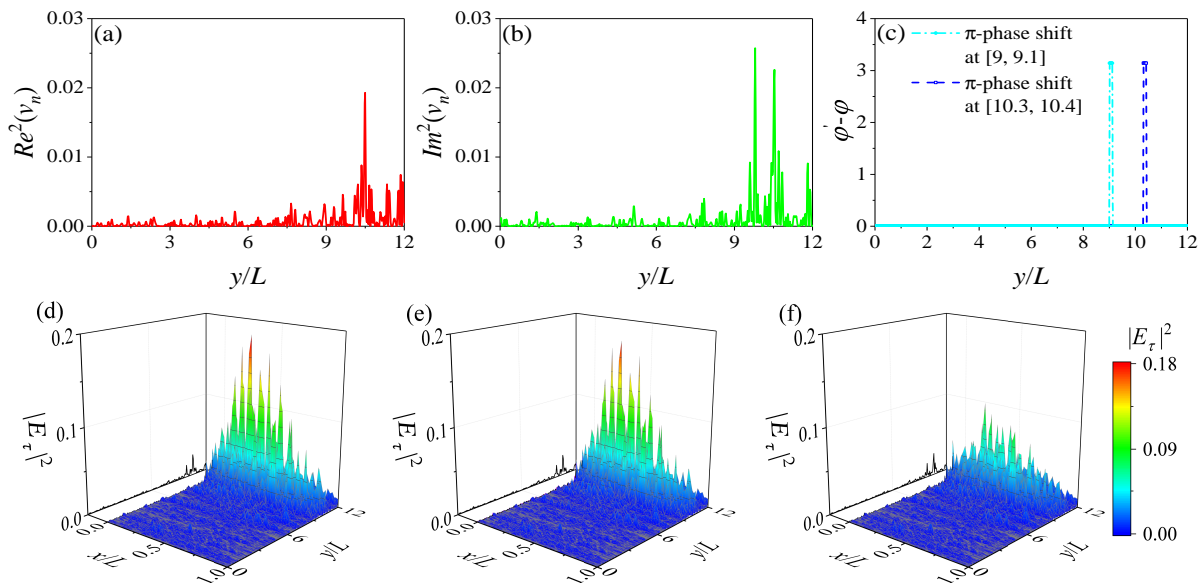


FIG. 4. A numerical example shows that the eigenvector $v_n(y)$ ($\tau_n = 1, N = 200$) is localized within the slab in the region of $9.5 \leq y/L \leq 12$ (a,b). This localization of $v_n(y)$ at the input edge leads to the localization of eigenchannel structure in the y direction in the interior of the medium (d). When the phase of $v_n(y)$ in the region of $9.0 \leq y/L \leq 9.1$ is twisted by π (c, dotted-dashed line), the eigenchannel structure is unaffected (e). Whereas if the π -phase twist is introduced in the region of $10.3 \leq y/L \leq 10.4$ (c, dashed line), the eigenchannel structure is significantly changed (f). In (d), (e) and (f) the localization structures of $|E_{\tau_n}(x=0, y)|^2$ at the input edge are also plotted (black solid lines) to guide the eye.

where $\delta\epsilon(x)$ represents the fluctuation of the dielectric constant. For each solution of Eq. (8) with a given Ω there is a specific transmittance $\mathcal{T}(\Omega)$. We define the resonance as a local maximum $\mathcal{T}(\Omega_n) \equiv \mathcal{T}_n$ of the transmittance spectrum $\{\mathcal{T}(\Omega)\}$, where Ω_n is the resonant frequency. The energy density of the field at the resonant frequency is defined as the resonance structure:

$$\tilde{I}_{\mathcal{T}_n}(x) \equiv |E_{\Omega_n}(x)|^2. \quad (9)$$

This is another key quantity which we will study below. It is important to note that contrary to the 2D eigenchannel structure, Eq. (6), where the frequency Ω is fixed, to obtain 1D resonant structures we need to sample the frequency so that the resonances can appear.

Below we will show that although the transmission eigenchannel in 2D media and the transmission resonance in 1D media are quite different physical entities, their energy density spatial distributions manifest rather surprising similarity.

III. EIGENCHANNEL STRUCTURE IN DIMENSION CROSSOVER

In this section, we study numerically the evolution of eigenchannel structures in the crossover from a quasi-1D ($L \gg W$) diffusive medium to a wide ($W \gtrsim L$) 2D diffusive slab. To simulate the crossover we increase W , while keeping L , Ω , and the strength of the disorder fixed.

Specifically, below we will study the energy density profiles both in 2D [Eqs. (5) and (6)] and in 1D [Eq. (9)].

A. Localization of right-singular vectors of the TM

To study the eigenchannel structure given by Eq. (5), we first perform a numerical analysis of the transmission eigenvalue spectrum $\{\tau_n\}$ and the right-singular vectors $\{v_n\}$ of the TM. We use Eq. (1) to simulate the wave propagation. In simulations, the disordered medium is discretized on a square grid, with the grid spacing being the inverse wave number in the background. The squared refractive index at each site fluctuates independently around the background value of unity, taking values randomly from the interval $[0.03, 1.97]$. For simulations, the standard recursive Green's function method^{20–22} is adopted. Specifically, we computed the Green's function between grid points $(x' = 0, y')$ and $(x = L, y')$. From this we obtained the TM \mathbf{t} , and then numerically performed the singular-value decomposition to obtain $\{\tau_n\}$, $\{v_n\}$ and $\{u_n\}$.

First, we found that regardless of the width W , (throughout this work we consider W, L much larger than the mean free path ℓ) the eigenvalue density averaged over a large ensemble of disorder configurations follows a bimodal distribution, which was found originally for quasi 1D samples^{11–13} and shown later to hold for arbitrary diffusive samples²³.

However, as we show below, the spatial structures of

$\{\mathbf{v}_n\}$ undergo drastic changes, when W increases. To be precise, let us define the inverse participation ratio:

$$\frac{1}{\xi(\tau)} \equiv \left\langle \int dy |v_n(y)|^4 \right\rangle_{\tau=\tau_n}, \quad (10)$$

where $\xi(\tau)$ characterizes the extension (in the y direction) of $v_n(y)$ with $\tau_n = \tau$. Here $\langle \dots \rangle_{\tau=\tau_n}$ stands for the average over a large number of right-singular vectors corresponding to the same τ in statistically equivalent disorder configurations (i.e., same W , L and disorder strength). The simulation results show that at a given W , $\xi(\tau)$ is practically independent of τ (Fig. 3, inset). Therefore, it is expedient to introduce a new inverse participation ratio:

$$\frac{1}{\xi'} \equiv \left\langle \int dy |v_n(y)|^4 \right\rangle, \quad (11)$$

where the average is over a number of right-singular vectors corresponding to different singular values (in statistically equivalent disorder configurations). We find that the ratio of ξ'/W has a tendency of decreasing to zero with $N \propto W$ (main panel). This implies that when the sample crosses over from quasi-1D waveguide to 2D slab geometry, the right-singular vectors undergo a delocalization-localization crossover. The localization structure of $|v_n(y)|^2$ in a slab is exemplified in Fig. 4. We are not aware of any reports on this result in the literature. It is important to remark that the localization here merely means that $|v_n(y)|^2$ takes a significant value in a small area of the cross section, i.e., $\xi' \ll W$, and ξ' can vary with W .

It is surprising that for large W , the field $v_n(y)$ exhibits localization. Below we show an even more surprising phenomenon, which occurs for large W . Namely, not only is the field at the input and at the output localized, but it also remains localized in the transverse direction along the entire sample. This fundamental feature actually makes an eigenchannel mimic a waveguide.

B. Localization of eigenchannel structures

We computed the Green's function between grid points $(x' = 0, y')$ and (x, y') , where $0 \leq x \leq L$. By using Eq. (4) we obtained the coordinate-dependent transfer matrix $\mathbf{t}(x)$, which is a generalization of \mathbf{t} . Substituting the simulation results of $\{\mathbf{v}_n\}$ obtained before and $\mathbf{t}(x)$ into Eqs. (5) and (6) we found the profile $|\mathbf{E}_{\tau_n}(x, y)|^2$. We repeated the same procedures for many disorder configurations, and also for different widths.

Figure 1 represents simulation results of 2D eigenchannel structures $|\mathbf{E}_{\tau_n}(x, y)|^2$ in a single disordered sample. We found that in wide enough 2D slabs (Fig. 1, $N = 100, 200$), the spatial structures of eigenchannels are localized in the transverse y direction regardless of the eigenvalues τ_n . To put this observation in a firmer level,

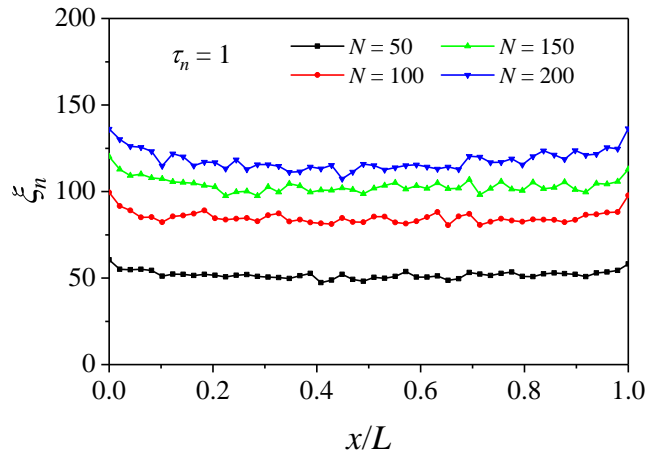


FIG. 5. Simulation results of the coordinate-dependent participation ratio $\xi_n(x)$ for different values of N .

we introduce the x -dependent inverse participation ratio:

$$\frac{1}{\xi_n(x)} \equiv \left\langle \frac{\int dy |\mathbf{E}_{\tau_n}(x, y)|^4}{(\int dy |\mathbf{E}_{\tau_n}(x, y)|^2)^2} \right\rangle \quad (12)$$

associated with the field distribution $\mathbf{E}_{\tau_n}(x, y)$ of the n th eigenchannel, where $\xi_n(x)$ characterizes the extension of the field distribution in the y direction at the penetration depth x , and the average is over a number of $\mathbf{E}_{\tau_n}(x, y)$ corresponding to the same singular value τ_n . Figure 5 presents typical numerical results of $\xi_n(x)$ for different values of N , from which it is easy to see that the field distribution is localized in the y direction for every x . In contrast, in a quasi-1D sample (Fig. 1, $N = 5$), no localization structures appear.

To understand the origin of the localization structures of eigenchannels, we modify the input field $\mathbf{v}_n \equiv \{v_n(y)\}$ (panels a and b in Fig. 4) to be $\mathbf{v}'_n \equiv \{v'_n(y)\}$ (panel c) in the following way. We twist by π the phase of $v_n(y) \equiv |v_n(y)|e^{i\varphi(y)}$ in certain region of y ,

$$v_n(y) \rightarrow v'_n(y) \equiv |v_n(y)| \exp\{i\varphi'(y)\}, \quad (13)$$

$$\varphi'(y) = \varphi(y) + \pi\chi(y), \quad (14)$$

where $\chi(y)$ takes the value of unity in the region, and otherwise of zero. Then we let this modified input field propagate in the medium, $\mathbf{v}'_n \rightarrow \mathbf{t}(x)\mathbf{v}'_n$, and compare the ensuing 2D energy density profile with the reference eigenchannel structure (panel d). We find that when the π -phase twist region is away from the localization center of $v_n(y)$ (panel c, dotted-dashed line), the resulting 2D energy density profile is indistinguishable from the reference eigenchannel structure (panel e). That is, the eigenchannel structure is insensitive to modifications. Whereas for the changes made in the localization center (panel c, dashed line), the ensuing energy density profile is totally different from the reference eigenchannel structure (panel f). This shows that the localization structures

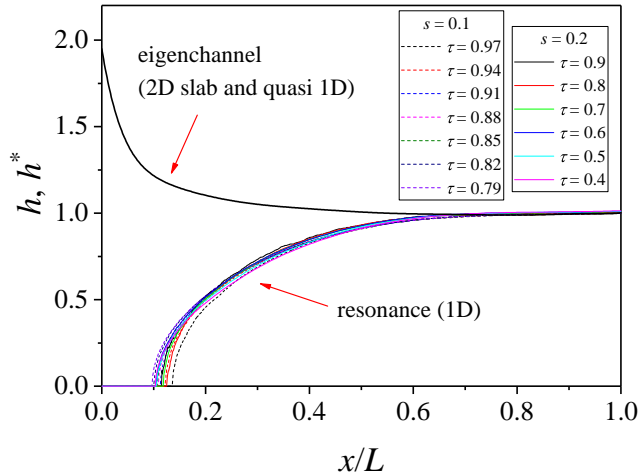


FIG. 6. Simulations of the resonance structures in 1D show that the h^* -function is universal with respect to both the resonant transmission \mathcal{T} and the disorder strength s . This property is similar to the universality of the h -function that determines the eigenchannel structures in 2D slabs and quasi 1D waveguides.

of $|\mathbf{E}_{\tau_n}(x, y)|^2$ are triggered by the localization structures of $v_n(y)$, as shown in Sec. III A, and are of wave-coherence nature.

C. Universality of eigenchannel structures in slabs

The localization of eigenchannel structures in the transverse direction implies that when a coherent wave is launched into a slab, it is decomposed into many partial waves, each of which propagates independently along an eigenchannel and whose energies cannot spread out of a specific region of the slab. The next question, naturally, is: how is the wave energy distributed inside a specific channel? In this part, we address this question, and analyze the connection of this distribution with the eigenchannel structure in a quasi 1D diffusive waveguide.

For a quasi-1D diffusive waveguide the ensemble average of $w_\tau(x)$, denoted as $W_\tau(x)$, is given by the following formula⁴:

$$W_\tau(x) = S_\tau(x)W_{\tau=1}(x), \quad (15)$$

where $W_{\tau=1}(x)$ is the profile corresponding to the transparent ($\tau = 1$) eigenchannel,

$$W_{\tau=1}(x) = 1 + \frac{\pi L x'(1-x')}{2\ell} \quad (16)$$

with $x' = x/L$, and

$$S_\tau(x) = 2 \frac{\cosh^2(h(x')(1-x')\phi)}{\cosh^2(h(x')\phi)} - \tau. \quad (17)$$

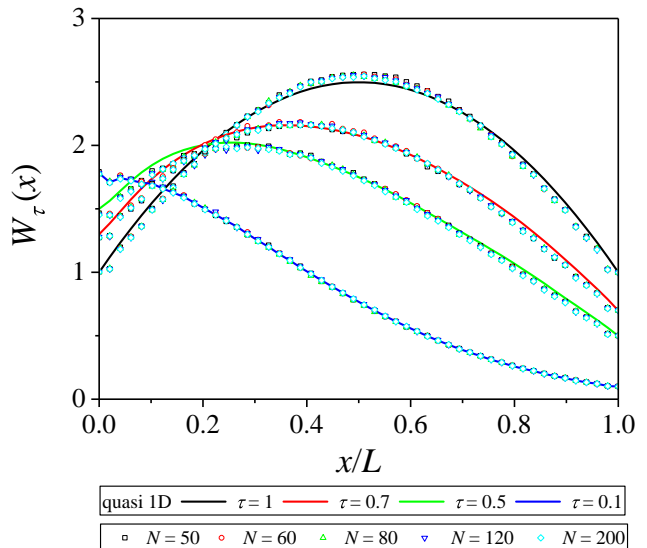


FIG. 7. Simulations show that for 2D slabs with different values of N , the ensemble averaged depth profile $W_\tau(x)$ (symbols) are well described by the analytic expression given by Eqs. (15)-(17) for quasi-1D waveguides (black solid lines). Note that at a given τ and x , all symbols for distinct N overlap. In simulations, L is fixed to be 50 and five ratios of W/L are considered, which are 3, 3.6, 4.8, 7.2 and 12, corresponding to $N = 50, 60, 80, 120$ and 200 , respectively.

Here we use

$$\tau = \frac{1}{\cosh^2 \phi}, \quad \phi \geq 0 \quad (18)$$

to parametrize the eigenvalue τ . Note that $h(x')$ is a function that increases monotonically from $h(1) = 1$ as x' decreases from 1, whose explicit form is given in Fig. 6 (black solid curve). Note that $h(x')$ is independent of N and τ .

Now we compare the eigenchannel structure in a slab with that in a quasi-1D waveguide described by Eqs. (15), (16) and (17). To this end we average 2000 profiles of $w_\tau(x)$ with the same or close eigenvalues τ . (Some of these eigenchannels may correspond to the same disorder configuration.) As a result, we obtain $W_\tau(x)$ for different values of τ , shown in Fig. 7. We see, strikingly, that for slabs with different number of N (i.e., width W) the structures of $W_\tau(x)$ are in excellent agreement with $W_\tau(x)$ described by Eqs. (15), (16) and (17).

IV. RESONANCE STRUCTURE

In the previous section, we have seen that in both 2D slabs and quasi-1D waveguides the ensemble averaged eigenchannel structure $W_\tau(x)$ is described by the universal formula Eqs. (15), (16) and (17). It is natural to ask whether this universality can be extended to strictly 1D

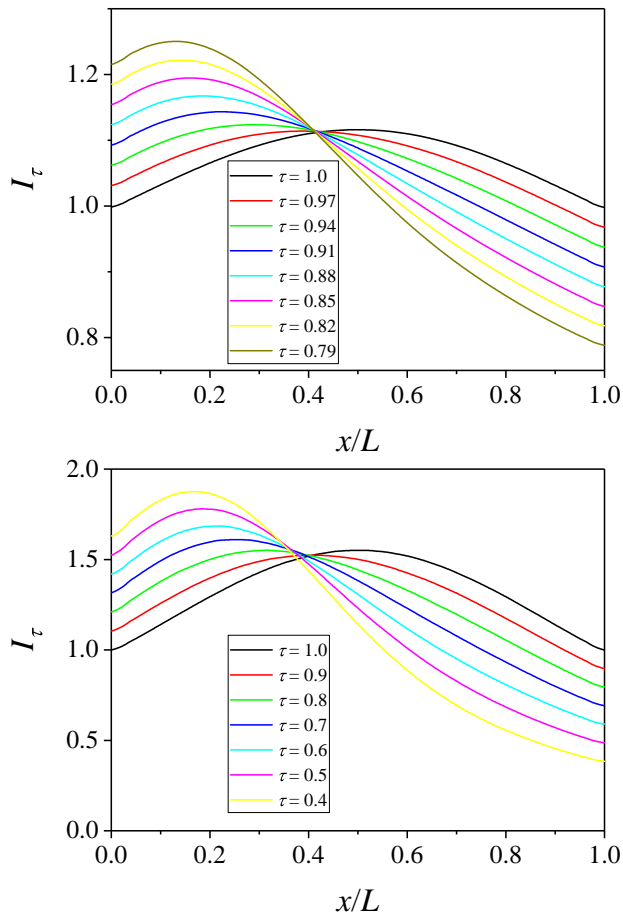


FIG. 8. The ensemble-averaged resonance structure $I_{\mathcal{T}}(x)$ for two different disorder strengths: $s = 0.1$ (top) and $s = 0.3$ (bottom), whose corresponding localization-to-sample length ratios are 12 and 3, respectively.

systems, in which the transmission eigenchannel does not exist. Noting that the resonant transmissions have the same bimodal statistics as the transmission eigenvalues of eigenchannels¹⁵, in this section we study numerically the resonance structure $\tilde{I}_{\mathcal{T}_n}(x)$. It is well known that in strictly 1D, there is no diffusive regime, because the localization length is of the order of mean free path²⁴. Instead, there are only ballistic and localized regimes. We consider the former below.

In simulations, the sample consists of 51 scatterers separated by 50 layers, whose thicknesses (rescaled by the inverse wave number in the background) are randomly distributed in the interval $d_0 \pm \delta$, with $d_0 = 10.0$ and $\delta = 9.0$. The sample length L is fixed to be $50d_0$. The scatterers are characterized by the reflection coefficients r_i between the neighbouring layers (i labels the scatterers.), which are chosen randomly and independently from the interval of $(-s, s)$, with $0 < s < 1$. The disorder strength is governed by s . We change the frequency Ω of incoming waves in a narrow band centered at Ω_0 and of half-width

$5\% \times \Omega_0$, and calculate the transmittance spectrum $\mathcal{T}(\Omega)$ by using the standard transfer matrix approach. We also change disorder configurations, so that for each resonant transmission \mathcal{T}_n , 5×10^5 profiles of $\tilde{I}_{\mathcal{T}_n}(x)$ are obtained. We then calculate the average of these profiles, denoted by $I_{\mathcal{T}_n}(x)$. Finally, we repeat the numerical experiments for different values of the disorder strength s .

Figure 8 shows the simulation results of $I_{\mathcal{T}}(x)$ for two different values of s . These profiles look similar to those presented in Fig. 7. For quantitative comparison, we compute the quantity $S_{\tau}^*(x) \equiv I_{\tau}(x)/I_{\tau=1}(x)$. Then, we present the function $S_{\tau}^*(x)$ in the form (recall that $x' = x/L$):

$$S_{\tau}^*(x) = 2 \frac{\cosh^2(h^*(x')(1-x')\phi)}{\cosh^2(h^*(x')\phi)} - \tau, \quad (19)$$

and find $h^*(x')$ for different values of τ and s from $S_{\tau}^*(x)$ calculated numerically (Fig. 6). The results are surprising: as shown in Fig. 6, $h^*(x')$ is a universal function, independent of τ and s , which is the key feature of $h(x')$ for eigenchannel structures. However, Fig. 6 also shows that the two universal functions, i.e., $h^*(x')$ and $h(x')$, are different. Therefore, allowing this minimal modification, the expression described by Eqs. (15), (16) and (17) is super-universal: it applies to both the resonance structure and the eigenchannel structure.

V. POSSIBLE APPLICATIONS

The universal properties of the transmission eigenchannels presented above open up outstanding possibilities to tailor the energy distribution inside higher-dimensional opaque materials, in particular, to concentrate energy in different parts of a diffusive sample. In the example shown in Fig. 9, two eigenchannels with low ($\tau_l = 0.1$) and high ($\tau_h = 1$) transmissions were excited, so that the input field had the form $\psi_{in} = \frac{1}{\sqrt{2}}(\mathbf{v}_h + \mathbf{v}_l)$. Here the right-singular vector $\mathbf{v}_{h(l)} \equiv \{v_{h(l)}(y)\}$ of the TM corresponds to a highly (low) transmitting eigenchannel. It is easy to see that the energy density profile generated by this input inside the medium is comprised of two phase coherent, but spatially separated parts. This is because the initial transverse localization of $\mathbf{v}_{h(l)}$ holds along the sample, and the integrated energy density profiles given by Eqs. (15), (16) and (17) have maxima at different points x (i.e., the higher is the transmission eigenvalue, the larger is the radiation penetration depth).

Simulations further show (Fig. 9) that it is possible, without changing the topology of the profile, to vary the relative intensity deposited in the two separated regions by simply modulating the phase field of ψ_{in} . For example, if we twist the phase $\varphi_l(y)$ of $v_l(y)$ at points y near the localization center [of $v_l(y)$] by π ,

$$v_l(y) \rightarrow v'_l(y) = |v_l(y)| \exp\{i\varphi'_l(y)\}, \quad (20)$$

$$\varphi'_l(y) = \varphi_l(y) + \pi\chi(y), \quad (21)$$

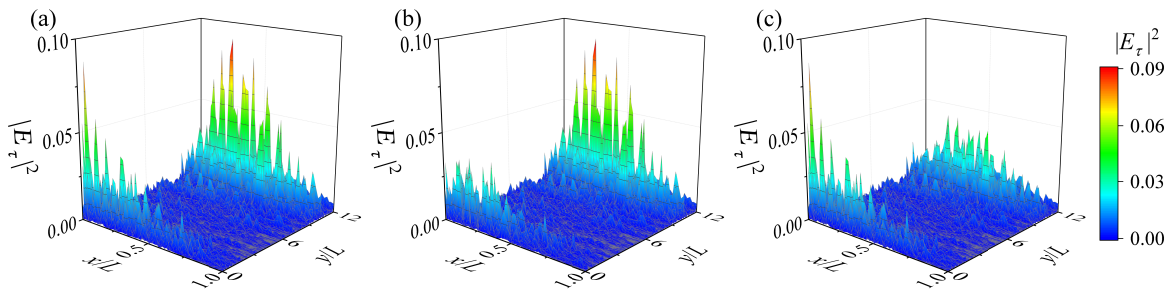


FIG. 9. Simulations show that by shaping the input field ψ_{in} , one can realize different profiles of energy density inside the medium. (a) The input field $\psi_{in} = \frac{1}{\sqrt{2}}(\mathbf{v}_h + \mathbf{v}_l)$, with $\mathbf{v}_{h(l)}$ corresponding to the right-singular vector of certain highly (low) transmitting eigenchannel. (b) The phase of \mathbf{v}_l is twisted by π in the region $0.3 \leq y/L \leq 0.4$. (c) The phase of \mathbf{v}_h is twisted by π in the region $10.3 \leq y/L \leq 10.4$.

where $\chi(y)$ takes the value of unity in a region near the localization center and otherwise is zero. For the ensuing input field $\psi_{in} = \frac{1}{\sqrt{2}}(\mathbf{v}_h + \mathbf{v}'_l)$, where $\mathbf{v}'_l \equiv \{v'_l(y)\}$, we find that the energy density deposited in the region corresponding to the low transmission eigenchannel is suppressed. Similarly, we can modify the input field to suppress the energy density deposited in the region corresponding to the high transmission eigenchannel.

VI. CONCLUSIONS AND OUTLOOK

Summarizing, we have shown that in a diffusive medium, as the medium geometry crosses over from quasi-1D structure to the structure of higher dimension, the incoming field given by the left-singular vector of the TM undergoes a delocalization-localization crossover, which results in the formation of a transverse-localized structure of the eigenchannel along the whole sample. At the same time, the longitudinal intensity distribution remains unchanged so that the depth profile $W_\tau(x)$ of the energy density of an eigenchannel with transmission τ is always described by Eqs. (15)-(17), regardless of medium geometry. The details of the system, such as the thickness and the disorder ensemble, only enter into the ratio of L/ℓ' in Eq. (15). This expression is super-universal, i.e., it encompasses not only the energy distributions in diffusive eigenchannels, but (with a minimal modification) the shape of the transmission resonances in strictly 1D random systems as well. These findings suggest that eigenchannels, which are the underpinnings of diverse diffusive wave phenomena in any dimension, might have a common origin, namely, 1D resonances. Although the similarity between the eigenchannel structure and the Fabry-Perot cavity has been noticed already in the pioneer study of eigenchannel structures², a comprehensive study of this phenomenon has not been carried out. While the fundamentals of this intriguing *local-*

ization phenomenon, which takes place *in the diffusive regime*, still remains to be explored in more depth, the results presented above may already be helpful in further advancing the methods of focusing coherent light through scattering media by wavefront shaping. Another area of potential applications is random lasing^{25,26} in diffusive media. Moreover, based on previous studies^{15,27-29}, we expect that controlling the reflectivities of the edges of a sample one can tune the intensity distributions in eigenchannels, not only in quasi-1D media, but in samples of higher dimensions as well. In the future, it is desirable to explore the super-universality of eigenchannel structures in high-dimensional media, where wave interference is strong, so that Anderson localization or an Anderson localization transition occurs.

ACKNOWLEDGEMENTS

We are grateful to A. Z. Genack for many useful discussions. Y. P. B. and V. F. would like to thank Institute of Theoretical Physics of Chinese Academy of Sciences for the hospitality during their visit. This work is supported by the National Natural Science Foundation of China (Grants No. 11535011 and No. 11747601). F.N. is supported in part by the: MURI Center for Dynamic Magneto-Optics via the Air Force Office of Scientific Research (AFOSR) (FA9550-14-1-0040), Army Research Office (ARO) (Grant No. W911NF-18-1-0358), Asian Office of Aerospace Research and Development (AOARD) (Grant No. FA2386-18-1-4045), Japan Science and Technology Agency (JST) (Q-LEAP program, ImPACT program, and CREST Grant No. JPMJCR1676), Japan Society for the Promotion of Science (JSPS) (JSPS-RFBR Grant No. 17-52-50023, and JSPS-FWO Grant No. VS.059.18N), RIKEN-AIST Challenge Research Fund, and the John Templeton Foundation.

* ct@itp.ac.cn

¹ S. Rotter and S. Gigan, Rev. Mod. Phys. **89**, 015005 (2017).

- ² W. Choi, A. P. Mosk, Q. H. Park, and W. Choi, *Phys. Rev. B* **83**, 134207 (2011).
- ³ M. Davy, Z. Shi, and A. Z. Genack, *Phys. Rev. B* **85**, 035105 (2012).
- ⁴ M. Davy, Z. Shi, J. Park, C. Tian, and A. Z. Genack, *Nat. Commun.* **6**, 6893 (2015).
- ⁵ S. F. Liew and H. Cao, *Opt. Express* **23**, 11043 (2015).
- ⁶ O. S. Ojambati, A. P. Mosk, I. M. Vellekoop, A. Lagendijk, and W. L. Vos, *Opt. Express* **24**, 18525 (2016).
- ⁷ R. Sarma, A. G. Yamilov, S. Petrenko, Y. Bromberg, and H. Cao, *Phys. Rev. Lett.* **117**, 086803 (2016).
- ⁸ M. Koirala, R. Sarma, H. Cao, and A. Yamilov, *Phys. Rev. B* **96**, 054209 (2017).
- ⁹ P. L. Hong, O. S. Ojambati, A. Lagendijk, A. P. Mosk, and W. L. Vos, *Optica* **5**, 844 (2018).
- ¹⁰ P. Fang, L. Y. Zhao, and C. Tian, *Phys. Rev. Lett.* **121**, 140603 (2018).
- ¹¹ O. N. Dorokhov, *Pis'ma Zh. Eksp. Teor. Fiz.* **36**, 259 (1982); [*JETP Lett.* **36**, 318 (1982)].
- ¹² O. N. Dorokhov, *Solid State Commun.* **51**, 381 (1984).
- ¹³ P. A. Mello, P. Pereyra, and N. Kumar, *Ann. Phys. (N.Y.)* **181**, 290 (1988).
- ¹⁴ C. W. J. Beenakker, *Rev. Mod. Phys.* **69**, 731 (1997).
- ¹⁵ L. Y. Zhao, C. Tian, Y. P. Bliokh, and V. Freilikher, *Phys. Rev. B* **92**, 094203 (2015).
- ¹⁶ K. Y. Bliokh, Y. P. Bliokh, and V. D. Freilikher, *J. Opt. Soc. Am. B* **21**, 113 (2004).
- ¹⁷ P. W. Anderson, *Phys. Rev.* **109**, 1492 (1958).
- ¹⁸ M. E. Gertsenshtein and V. B. Vasil'ev, *Teor. Veroyatn. Primen.* **4**, 424 (1959) [*Theor. Probab. Appl.* **4**, 391 (1959)].
- ¹⁹ K. Yu. Bliokh, Yu. P. Bliokh, V. Freilikher, S. Savel'ev, and F. Nori, *Rev. Mod. Phys.* **80**, 1201 (2008).
- ²⁰ H. U. Baranger, D. P. DiVincenzo, R. A. Jalabert, and A. D. Stone, *Phys. Rev. B* **44**, 10637 (1991).
- ²¹ A. MacKinnon, *Z. Phys. B* **59**, 385 (1985).
- ²² G. Metalidis and P. Bruno, *Phys. Rev. B* **72**, 235304 (2005).
- ²³ Yu. V. Nazarov, *Phys. Rev. Lett.* **73**, 134 (1994).
- ²⁴ V. L. Berezinskii, *Zh. Eksp. Teor. Fiz.* **65**, 1251 (1973) [*Sov. Phys. JETP* **38**, 620 (1974)].
- ²⁵ H. Cao, Y. G. Zhao, S. T. Ho, E. W. Seelig, Q. H. Wang, and R. P. H. Chang, *Phys. Rev. Lett.* **82**, 2278 (1999).
- ²⁶ D. S. Wiersma, *Nature Phys.* **4**, 359 (2008).
- ²⁷ X. J. Cheng, C. S. Tian, and A. Z. Genack, *Phys. Rev. B* **88**, 094202 (2013).
- ²⁸ D. Akbulut, T. Strudley, J. Bertolotti, E. P. A. M. Bakkers, A. Lagendijk, O. L. Muskens, W. L. Vos, and A. P. Mosk, *Phys. Rev. A* **94**, 043817 (2016).
- ²⁹ X. Cheng, C. Tian, Z. Lowell, L. Y. Zhao, and A. Z. Genack, *Eur. Phys. J. Special Topics* **226**, 1539 (2017).